ACS APPLIED NANO MATERIALS

www.acsanm.org Article

Multiwalled Carbon Nanotubes Coated with Nitrogen–Sulfur Co-Doped Activated Carbon for Detecting Fenitrothion

Krishna Jangid, Rakesh P. Sahu, Richa Pandey, Ri Chen, Igor Zhitomirsky, and Ishwar K. Puri*

Cite This: *ACS Appl. Nano Mater.* 2021, 4, 4781–4789 Read Online

ACCESS | Metrics & More | Article Recommendations | Supporting Information

ABSTRACT: A nonenzymatic electrochemical sensor is drop casted for sensitive and specific fenitrothion (FT) detection, where a glassy carbon electrode (GCE) is modified by depositing an ink containing nitrogen–sulfur co-doped activated carbon-coated multiwalled carbon nanotubes (NS-AC-MWCNTs). We provide a method for NS-AC-MWCNT synthesis as follows. First, polypyrrole is coated on multiwalled carbon nanotubes (PPy-MWCNT). Then, the PPy coating is carbonized and chemically activated to enhance the specific surface area. The activated carbon coating, co-doped with nitrogen–sulfur, improves its surface electrical conductivity and electrocatalytic response as an electrode. Electrochemical impedance spectroscopy (EIS) confirms enhanced charge transfer for the NS-AC-MWCNT/GCE in comparison with MWCNT/GCE and GCE. Scanning electron microscopy (SEM) and high-resolution transmission electron microscopy (HRTEM) with fast Fourier transform (FFT) elucidate the morphology of the material, and X-ray photoelectron spectroscopy (XPS) and Raman spectroscopy its chemical and structural characteristics. An NS-AC-MWCNT-containing ink is prepared and deposited on a GCE to fabricate a sensor to detect FT. The volume of NS-AC-MWCNT ink deposited, buffer solution pH, accumulation potential V_{pp} and time t_{pp}, and square wave voltammetry (SWV) parameters are optimized. For 0.05–40 μM FT concentrations, the sensor provides a linear current response with a 4.91 nM limit of detection (LOD) with a signal-to-noise (S/N) ratio of 3. Chemical interferents have negligible influence on FT detection. The sensor detects FT in real lake and tap water samples.

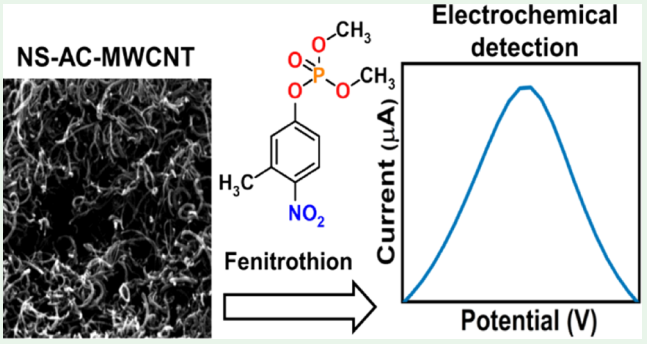

KEYWORDS: *fenitrothion, organophosphates, square wave voltammetry, carbon nanotube, nitrogen–sulfur doping, activated carbon, nonenzymatic sensor*

INTRODUCTION

The use of pesticides to control weeds, insect infestations, and diseases has increased steadily to meet rising global food demand, contributing to pesticide accumulation in the environment that is harmful to humans and other life forms.[1] Pesticide runoff contaminates surface and groundwater, increasing its toxicity toward microorganisms, which reduces soil fertility.[2,3] Since their introduction in the 1960s, the consumption of organophosphorus compounds (OP) that replace dichlorodiphenylytrichloroethane (DDT) has consistently increased.[4] Used in agricultural fields, gardens, and commercial areas, OP are the most used pesticides, contributing 70% toward overall pesticide consumption.[5,6] Continuous OP exposure produces severe and fatal physiological effects in humans, including mental disorders such as depression, anxiety, headache, blurred vision, nausea, vomiting, lowered heart rate, loss of coordination, fever, coma, and death.[7] The World Health Organization reports that over 750 000 people suffer from pesticide poisoning yearly, of whom 350 000 die.[8] Human pesticide poisonings and related illness are estimated to have an annual economic cost of $1 billion in the United States alone.[9]

Several analytical methods are used to detect OP, including gas or high-performance liquid chromatography[10] and mass spectrometry.[11] These techniques are typically complicated, costly, and require complex sample procedures and trained professionals to operate, limiting their operation in field conditions.[12] An electroanalytical method based on inhibition of immobilized acetylcholinesterase (AChE) enzyme[13,14] is used for rapid on-site pesticide analysis. However, it cannot provide real-time pesticide analysis with confidence because of the poor chemical and physical stability of enzymes due to their denaturation, sensitivity to the chemical environment

Received: February 5, 2021
Accepted: April 21, 2021
Published: May 5, 2021

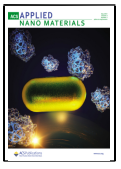

https://doi.org/10.1021/acsanm.1c00376
ACS Appl. Nano Mater. 2021, 4, 4781–4789

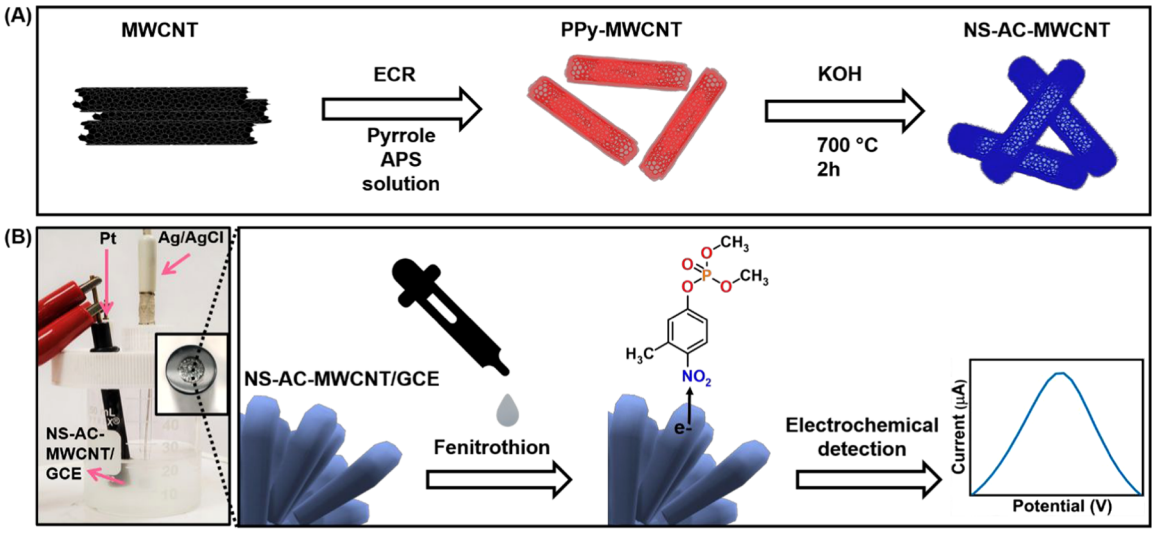

Figure 1. (A) Schematic of NS-AC-MWCNT synthesis, where prepared PPy-coated MWCNTs are activated with KOH and carbonized at 700 °C. (B) Schematic of the sensor fabrication. NS-AC-MWCNT modification of GCE is performed with drop casting the ink on GCE which is used to detect FT in ABS via SWV.

(e.g., pH), and chemical degradation during fabrication, storage, and use.[15]

The sensitivity of an electroanalytical sensor is influenced by its specific surface area, electrical conductivity, thereby the electrocatalytic property of the working electrode.[16−19] The higher surface area available with nanomaterials amplifies the analyte signal response. Carbon nanomaterials (e.g., carbon nanotubes and graphene), conductive polymers (e.g., PANI, PEDOT, and polypyrrole), and metal nanoparticles (e.g., Au, Ag, and Pt) have been investigated in this regard.[20−22] Porous materials, such as activated carbon (AC), with a higher available surface area, are used to detect heavy metal ions, e.g., Cd(II), Pb(II), Cu(II), and Hg(II).[23] The conductivity of porous carbon materials can be increased with heteroatom doping.[24−28] The nitrogen−sulfur co-doping of AC also supplies additional valence electrons and enhances conductivity. Since it is more electronegative than carbon, nitrogen doping polarizes surrounding carbon atoms, enhancing their electrocatalytic activity through a higher charge density. The atomic size difference between sulfur and carbon changes interlayer spacing and orbital matching in AC, creating additional active sites that enhance its electrocatalytic behavior.[29]

Our objective is to synthesize and fabricate AC-coated MWCNTs for detecting organophosphates with low resistance and high sensitivity. We hypothesize that the activated carbon coating co-doped with nitrogen−sulfur on multiwalled carbon nanotubes increases both the surface area and surface electrical conductivity. Concisely, MWCNTs act as a supporting structure for the NS-AC coating, where AC-coated MWCNTs provide a higher electroactive surface area, enhancing the number of active sites available for OP detection. NS co-doping of AC improves the electrical conductivity of the electrode surface and promotes faster charge transfer between FT and the electrode. The enhanced electrocatalysis provides the motivation for modifying a glassy carbon electrode (GCE) to detect OP. Hence, we synthesize a novel nitrogen−sulfur co-doped activated carbon-coated multiwalled carbon nanotube (NS-AC-MWCNT) composite and deposit it in the form of an ink over GCE to fabricate a sensor that serves as an electrode to detect the OP surrogate fenitrothion (FT) with SWV.

The synthesis of N-AC-MWCNT has been accomplished by carbonizing PPy-MWCNT, prepared using cetrimonium bromide (CTAB) and ammonium persulfate (APS) as dispersant and oxidant, respectively.[30,31] Sulfur and nitrogen co-doped carbon nanotubes were synthesized using methyl orange as a dopant and aniline as a nitrogen source.[32] We have a conceptually different approach by utilizing pyrrole as the nitrogen source and eriochrome cyanine (ECR) as the multifunctional dopant to prepare our material. ECR has advantages over CTAB and methyl orange, since the structure of the aromatic compound promotes carbon nanotube adsorption, and the charged groups promote electrostatic repulsion between the nanotubes, improving nanotube dispersion. Charged groups on aromatic compound are also beneficial for polymerization. Therefore, as a multifunctional dopant, ECR provides better nanotube dispersion and a better polypyrrole coating.[33,34]

Below, we (1) describe the synthesis of NS-AC-MWCNT by carbonizing PPy-MWCNT prepared with ECR and APS, a new method to fabricate a composite that has higher conductivity and surface area for effective electrochemical sensing; (2) report the first use of an NS-AC-MWCNT ink to detect FT with square wave voltammetry; (3) characterize the influence of the amount of ink deposited on the GCE, buffer solution pH, accumulation potential and time, and SWV parameters on the wave shape and current response of the FT sensor; (4) confirm sensor sensitivity and specificity for FT detection; (5) confirm the use of the sensor to detect FT in real lake and tap water samples; and (6) compare the sensing performances of differently modified electrodes.

MATERIALS AND METHODS

Chemicals and Instruments. Fenitrothion (FT, analytical grade), pyrrole (Py, purity >98%, stored at 4 °C before use), sodium acetate buffer solution (ABS, molecular biology grade), potassium hydroxide (KOH), dichlorvos, chlorpyrifos, ammonium persulfate (APS), and eriochrome cyanine (ECR) were purchased from Sigma-Aldrich (Canada). Multiwalled carbon nanotubes (MWCNTs) with an outside diameter of 13 nm, inner diameter of 4 nm, and lengths

https://doi.org/10.1021/acsanm.1c00376
ACS Appl. Nano Mater. 2021, 4, 4781−4789

between 1 and 2 μm were obtained from Bayer Inc. (Germany). Deionized water (DI) and all reagents were used without further modification. The pH of the buffer solution was adjusted using a pH meter with 0.1 M NaOH and 0.1 M HCl solutions. Stock solutions of FT were prepared in ethanol and stored in a refrigerator at 4 °C before use. Laboratory tap water and Lake Ontario lake water from Bayfront Park in Hamilton, Canada, were used as is to detect spiked FT.

Cyclic voltammetry (CV), square wave voltammetry (SWV), and electrochemical impedance spectroscopy (EIS) were performed with a PARSTAT 2273 potentiostat (Princeton Applied Research) using its conventional three-electrode configuration that consists of a glassy carbon electrode as the bare working electrode, platinum wire as counter electrode, and Ag/AgCl as reference electrode, all immersed in ABS. Chemical analysis was performed by XPS (Physical Electronics, model Quantera II) with a monochromatic Al Kα X-ray source at 1486.6 eV. Raman spectroscopy was conducted with a Renishaw inVia spectrometer at a 514 nm laser excitation by drop-casting 4 μL of the sample on a glass substrate. The synthesized material was characterized by SEM (JEOL 6610LV), HRTEM (FEI Titan 80-300 LB), and FFT performed with ImageJ software.

Synthesis of PPy-Coated MWCNT. Polypyrrole (PPy)-coated MWCNTs were synthesized through chemical polymerization[35,36] utilizing APS as oxidant and ECR as a dopant for Py and dispersant for MWCNTs,[33] as shown in the schematic in Figure 1A. Two hundred milligrams of MWCNTs were homogenously suspended with ultrasonication in 20 mg of ECR dissolved in 200 mL of DI water. The resulting suspension was stirred at 4 °C in an ice bath to which 800 mg of Py was added. Typically, 3.4 g of APS was dissolved in 15 mL of DI water, added to the MWCNT suspension, and stirred for 20 h in an ice bath at 4 °C. The synthesized material was washed with DI water and dried in an oven at 70 °C.

Synthesis of NS-AC-MWCNT. Nitrogen−sulfur co-doped activated carbon-coated MWCNT (NS-AC-MWCNT) was synthesized through chemical activation and carbonization (Figure 1A).[30,31] After synthesis, 1 g of PPy-coated MWCNT was dispersed in 25 mL of 4 M KOH and the suspension was stirred and dried in air at 80 °C to form a powder. The powder was activated and carbonized under a nitrogen atmosphere in a tube furnace, first at 700 °C for 2 h and then cooled to room temperature. The resulting filtrate was made pH neutral by washing it with 1 M HCl and DI water after which it was dried for 12 h in an oven at 70 °C. The synthesized NS-AC-MWCNT material was dispersed in ethanol to form a uniform 1 mg/mL suspension. Different deposition volumes of the material were drop cast on GCE and dried in air to obtain electrodes.

The fabrication of the NS-AC-MWCNT/GCE electrochemical sensor is illustrated in Figure 1B. The electrodes were electrochemically activated by successively scanning them in an acetate buffer (pH 5) from 0.1 to 1.2 V (at a scan rate of 100 mV/s) until stabilized. CV or SWV were utilized to obtain the current response of FT. CVs were scanned for 50 μM FT in a 0.2 M acetate buffer (pH 5.0) at a scan rate of 50 mV/s between −0.8 and 0.5 V vs Ag/AgCl. CV was also performed to determine the electroactive surface area of different electrodes in 1 mM $Fe(CN)_6^{3-}/Fe(CN)_6^{4-}$/0.1 M KCl solution for scan rates from 25 to 200 mV/s. SWV was performed in 0.2 M acetate buffer to determine the optimum amount of NS-AC-MWCNT deposited, pH of the acetate buffer, accumulation potential, accumulation time, and SWV parameters, such as amplitude, step potential, and frequency. SWV was utilized to analyze the FT response. The optimized SWV conditions were a 10 Hz frequency, 10 mV step potential, and 140 mV amplitude. The limit of detection (LOD) of the sensor was calculated from standard deviation σ of the current response of the NS-AC-MWCNT/GCE in ABS at optimized conditions when no FT was present and the slope of the linear regression fit of the calibration curve m for samples containing FT using the formula LOD = $3\sigma/m$.[37] Sensor selectivity was examined by introducing 10-fold excess concentrations, i.e., 200 μM, above the FT concentration of nine commonly found salt interferents and organophosphates (dichlorvos and chlorpyrifos) in drinking or usable water. The salts were of Ni^{2+} ($NiSO_4{\cdot}6H_2O$), Zn^{2+} ($ZnSO_4{\cdot}7H_2O$), Mn^{2+} ($Mn(CH_3COO)_2{\cdot}4H_2O$), Co^{2+} ($CoSO_4{\cdot}7H_2O$), Fe^{3+} ($H_2Fe_2O_{13}S_3$), Cl^- (NaCl), PO_4^{3-} (Na_3PO_4), NO_3^- (KNO_3), and SO_4^{2-} (K_2SO_4), in 20 μM of FT in ABS. Lake water was filtered with 8 μm pore size filter paper. Thereafter, 0.2 M (pH = 5) solutions of lake water and laboratory tap water samples were obtained by adding 2 mL of 2 M acetate buffer to each 18 mL of sample. These samples were spiked with known concentrations of FT and a linear regression fit used to calculate the FT concentration.

RESULTS AND DISCUSSION

Material Characterization. The morphology of the synthesized NS-AC-MWCNT is observed from SEM and HRTEM images and FFT sample analysis. Figure 2A presents

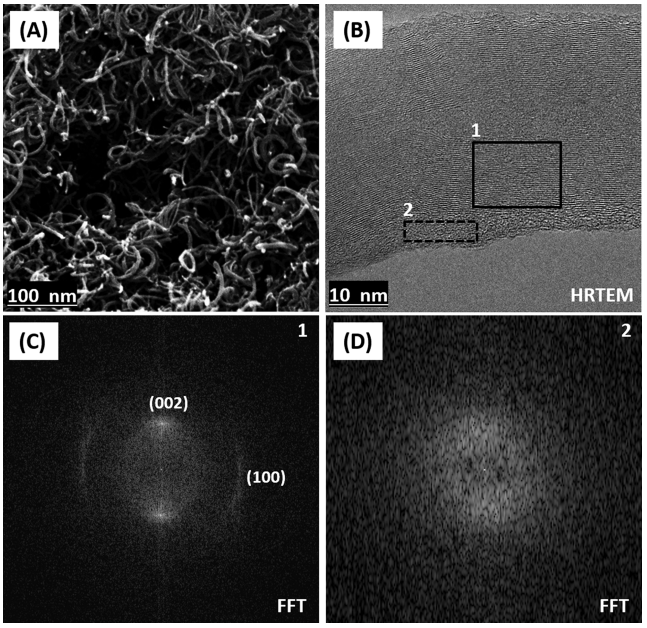

Figure 2. Morphological characterization of the composite material: (A) SEM and (B) HRTEM images, and (C, D) FFT images of the marked regions in the HRTEM image. The crystalline (C) and amorphous (D) locations are identified by solid and dashed lines in (B) that correspond to the carbon nanotubes and activated carbon coating.

an SEM image that shows the microstructure of the randomly interconnected nanotubes forming a spongelike architecture, illustrating the three dimensionalities of the material. Carbonization of PPy-coated MWCNT produces AC-coated MWCNT.[30,31] Figure 2B shows an HRTEM image of the NS-AC-MWCNT with the region of crystalline carbon nanotube and amorphous coating of AC on MWCNT being marked by solid and dashed lines, respectively. The FFT analysis[38] of the marked regions in the HRTEM image is presented in Figure 2C,D. Well-defined spots in Figure 2C correspond to the (002) and (100) crystalline planes of carbon nanotube.[39] Blurred spots correspond to the amorphous activated carbon coating on the outer surfaces of the nanotubes (Figure 2D). The obtained core−shell architecture of the AC-coated MWCNT is in agreement with the previously reported work.[41]

The XPS survey spectra in Figure 3A show weak peaks for K 2s and K 2p that occur due to KOH treatment of the PPy-MWCNT, as well as peaks for C 1s, O 1s, O Kll, S 1s, S 2p, and N 1s. Elemental composition from the XPS data reveals that carbon, nitrogen, sulfur, oxygen, chlorine, and potassium

https://doi.org/10.1021/acsanm.1c00376
ACS Appl. Nano Mater. 2021, 4, 4781−4789

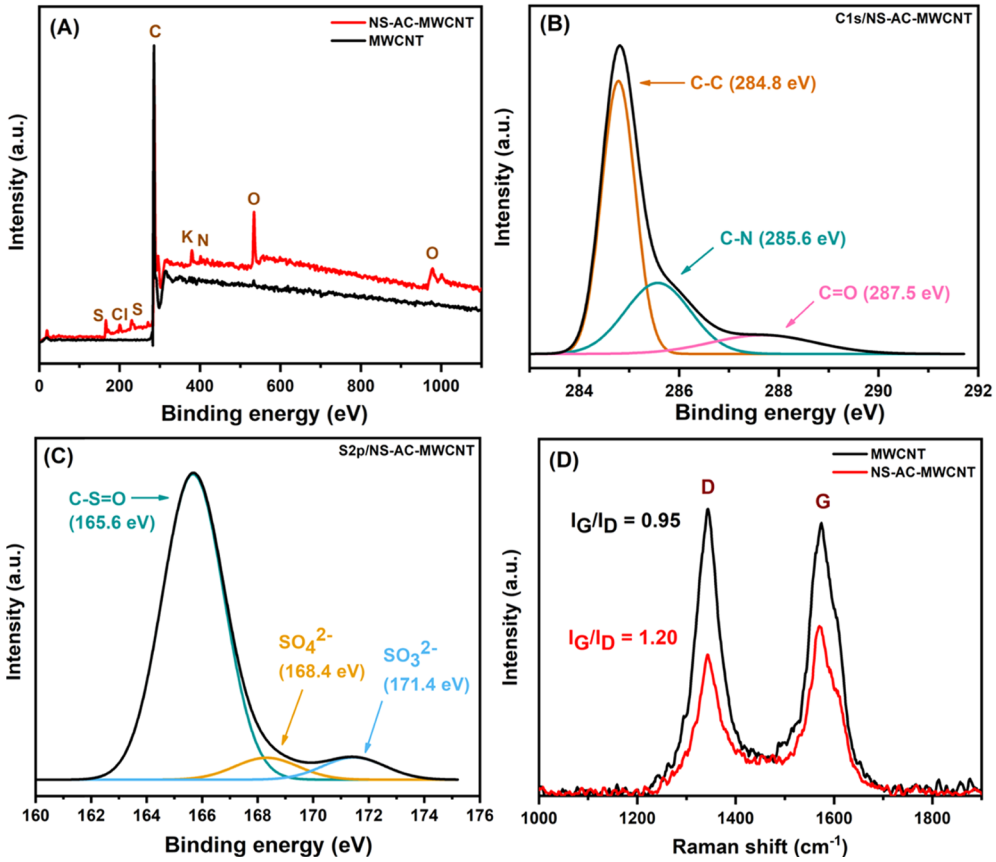

Figure 3. (A) XPS survey spectra for NS-AC-MWCNT and pristine MWCNT. (B, C) Higher-resolution XPS spectra for N 1s and S 2p for NS-AC-MWCNT confirm nitrogen- (N-5, N-6, and N-Q) and sulfur-comprising groups (sulfoxide, sulfate, and sulfite). (D) Raman spectra for pristine MWCNT and NS-AC-MWCNT reveal D and G bands, where the intensity ratio of the G band to D band I_G/I_D indicates the degree of graphitization.

in NS-AC-MWCNT are present in 78.7, 2.3, 2.3, 10.6, 1.2, and 5.1 wt %, respectively (Table S1). The higher-resolution N 1s spectrum of Figure 3B reveals peaks at 398.4, 400.2, and 400.9 eV corresponding to the N-6 (pyridinic), N-5 (pyrrolic), and N-Q (quaternary) nitrogen groups, respectively.[30,40] Quaternary and pyridinic nitrogen groups have a strong electron donor tendency[41] that enhances electron transfer and improves sensor sensitivity. In addition to the C−C (284.7 eV), C−OH (285.7 eV), C═O (287.4 eV), and COOH (290.8 eV) peaks of C 1s of MWCNT (Figure S1A), the NS-AC-MWCNT spectrum provides another C−N (285.6 eV) peak with C−C (284.8 eV) and C═O (287.5 eV) peaks (Figure S1B) that correspond to nitrogen doping.[30] The S 2p spectra of Figure 2C contain peaks at 165.7, 168.4, and 171.4 eV for sulfoxide, sulfate, and sulfite groups[42] that confirm sulfur doping. PPy served as a source for nitrogen-containing groups, while multifunctional dopant, ECR and oxidant, APS served as the sources for sulfur-containing groups. The O 1s spectra for both MWCNT (Figure S1C) and NS-AC-MWCNT (Figure S1D) show oxygen-containing C═O, C−OH, and COOH groups.

Raman spectroscopy reveals the degree of ordered structure, defects, and hybridization[43,44] and evaluates the extent of graphitization that influences the electrical conductivity.[45,46] Raman spectra for MWCNT and NS-AC-MWCNT (Figure 2D) show two peaks at 1343.5 and 1574.1 cm^{-1} for the D and G bands, respectively, where the D band is associated with disordered carbon (sp^3) and the G band with graphitic carbon (sp^2).[43] The intensity ratio I_G/I_D is indicative of the degree of graphitization. For MWCNT and NS-AC-MWCNT, I_G/I_D = 0.95 and 1.20, respectively, confirming the enhancement of graphitization, thereby electrical conductivity, in the latter composite material.

The electrochemical response of synthesized NS-AC-MWCNT composite is investigated using CV, SWV, and EIS to understand the effect of different modifications on the charge transfer at the electrode−electrolyte interface. Figure 4A shows the electrochemical impedance data in the Nyquist plot. Nyquist plots for GCE, MWCNT/GCE, and NS-AC-MWCNT/GCE are fitted per Randles equivalent circuit model.[47] The charge transfer resistance is calculated from the experimental data and the analysis of the equivalent circuit. There is a significant decrease in the charge transfer resistance R_{ct} at the interface of electrolyte and electrode surface when the GCE is coated with MWCNT, where R_{ct} = 49.4 Ω for GCE and 12.6 Ω for MWCNT/GCE. This R_{ct} decrease occurs due to the higher electrical conductivity and surface area for the MWCNT with respect to the GCE.[48,49] For the NS-AC-MWCNT/GCE, R_{ct} further decreases to 5.4 Ω. This significant decrease in resistance is attributed to the associated increase in the electrochemically active surface area, therefore active sites available for FT detection, and electrical conductivity, thereby enhancing electrocatalysis by the NS-AC-MWCNT-modified GCE.

The interaction of FT and the NS-AC-MWCNT is investigated with CV and SWV. We suggest $\pi-\pi$ interactions are involved between FT and electrode. These interactions

https://doi.org/10.1021/acsanm.1c00376
ACS Appl. Nano Mater. 2021, 4, 4781−4789

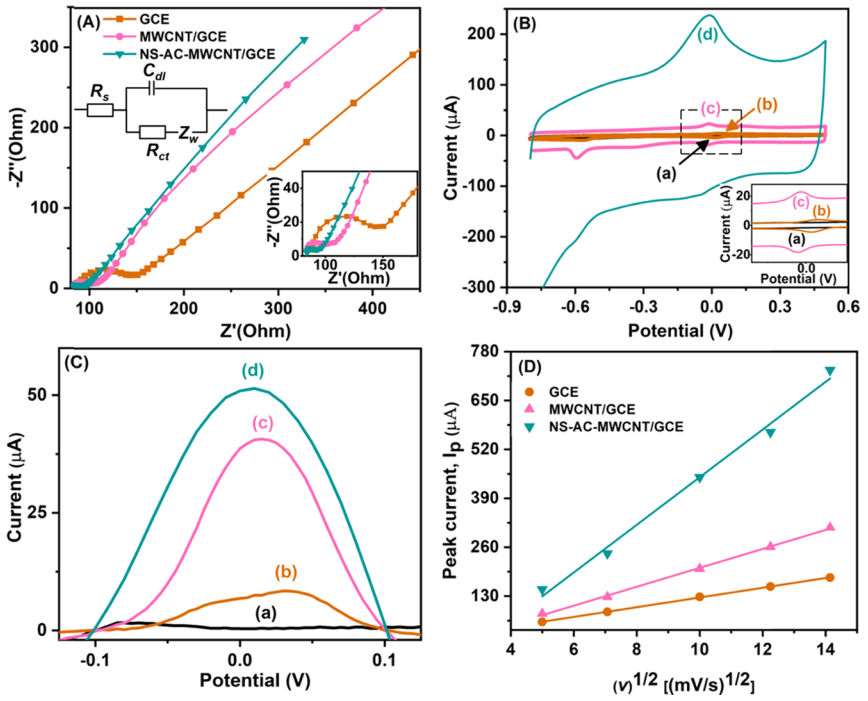

Figure 4. Electrochemical characterization of the sensor. (A) Nyquist plot for the three-electrode modifications in a 1 mM $Fe(CN)_6^{3-}$/$Fe(CN)_6^{4-}$/0.1 M KCl solution (0.1−10^5 Hz, 5 mV). The inset shows the higher frequency range of the Nyquist plot for differently modified working electrodes: R_s, R_{ct}, C_{dl}, and Z_w denote electrolyte resistance, charge transfer resistance, double-layer capacitance, and Warburg impedance, respectively. (B) Comparison of the cyclic voltammograms for (a) GCE in the absence of fenitrothion with (b) GCE, (c) MWCNT/GCE, and (d) NS-AC-MWCNT for 50 μM FT in 0.2 M acetate buffer solution (pH 5.0) at a scan rate of 50 mV/s. (C) SWVs for GCE (a: FT absent, b: FT present), and for (c) MWCNT/GCE and (d) NS-AC-MWCNT/GCE with 50 μM FT in 0.2 M acetate buffer solution (pH 5.0) at a scan rate of 50 mV/s. (D) Plots of I_p vs $\nu^{1/2}$ obtained from cyclic voltammograms of GCE, MWCNT/GCE, and NS-AC-MWCNT/GCE in 1 mM $Fe(CN)_6^{3-}$/$Fe(CN)_6^{4-}$/0.1 M KCl solution at scan rates: 25, 50, 100, 150, and 200 mV/s.

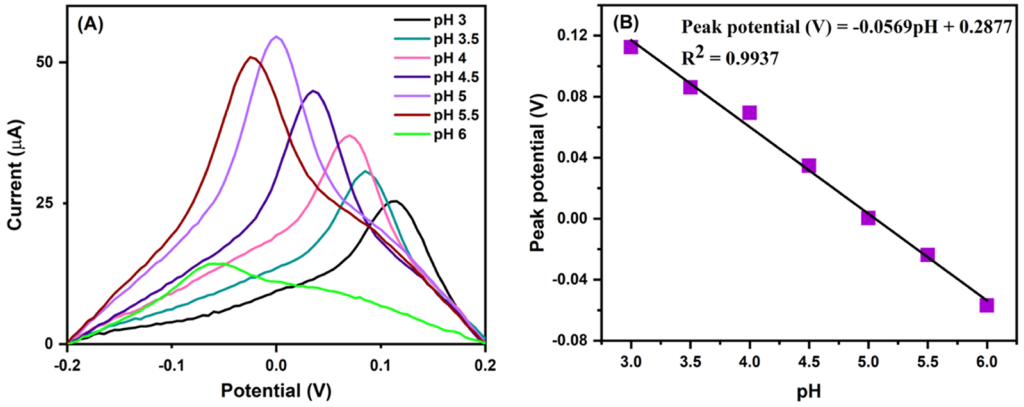

Figure 5. (A) Effect of pH on the SWV for 50 μM fenitrothion with an NS-AC-MWCNT-modified GCE in 0.2 M acetate buffer solution. (B) Plot of peak potential (V) vs pH of the 0.2 M acetate buffer for 50 μM fenitrothion.

further facilitate the charge transfer by enhancing the reduction and oxidation capabilities of the electrode for the $-NO_2$ group on FT. Under a formal potential, the $-NO_2$ group first undergoes an irreversible reduction to the −NHOH group at a negative cathode potential of −0.59 V vs Ag/AgCl, followed by a reversible oxidation at −0.005 V vs Ag/AgCl and reduction of the −NO group at −0.06 V vs Ag/AgCl during the subsequent reverse scan,[22] as shown in Figure 4B and Schematic S1 in the Supporting Information.

The CV and SWV electrochemical profiles for NS-AC-MWCNT/GCE in the presence of FT are compared with profiles for GCE and MWCNT/GCE under similar conditions in Figure 4B,C. Compared to MWCNT/GCE, coating the MWCNT with nitrogen−sulfur co-doped activated carbon enhances the Faradaic current due to the higher electrocatalytic behavior of the modified electrode as discussed above. The electroactive surface areas of the GCE and modified electrodes with MWCNT and NS-AC-MWCNT were evaluated with CV using the Randles−Sevcik equation[18]

$$I_p = 2.69 \times 10^5 n^{3/2} A C D^{1/2} \nu^{1/2}$$

where I_p denotes anodic peak current, n number of electrons, A electroactive surface area, C concentration of $Fe(CN)_6^{3-}$/$Fe(CN)_6^{4-}$, D diffusion coefficient, and ν scan rate. CV measurements are performed in a 1 mM $Fe(CN)_6^{3-}$/

https://doi.org/10.1021/acsanm.1c00376
ACS Appl. Nano Mater. 2021, 4, 4781−4789

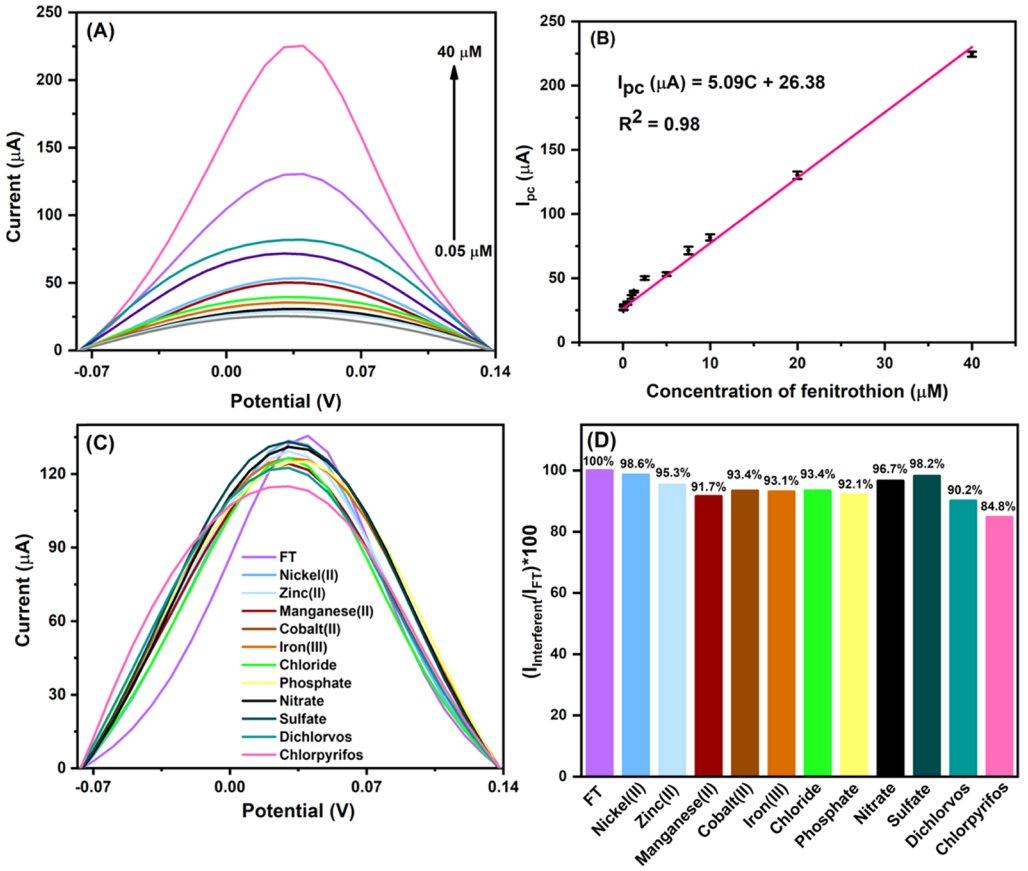

Figure 6. (A) SWVs for 0.05−40 μM fenitrothion concentrations measured with the NS-AC-MWCNT-modified GCE in 0.2 M acetate buffer solution at pH = 5. (B) Calibration of I_{pc} (peak current, μA) vs FT concentration (μM) detected by the sensor. (C) Sensor SWV response to 20 μM FT concentration at pH = 5 in ABS in the presence of different 200 μM (10× or 10-fold) concentrations of interferent species. (D) Percentage change in the current response to the FT solution spiked with different interferent species with respect to the response toward FT alone, i.e., in the absence of interferents.

$Fe(CN)_6^{4-}$/0.1 M KCl solution for scan rates of 25, 50, 100, 150, and 200 mV/s. Figure 4D shows the anodic peak current (I_p) vs square root of scan rate ($\nu^{1/2}$) for the GCE, MWCNT/GCE, and NS-AC-MWCNT/GCE. From the slope of I_p vs $\nu^{1/2}$, the surface areas of the GCE, MWCNT/GCE, and NS-AC-MWCNT/GCE electrodes are determined as 0.019, 0.037, 0.094 cm^2, respectively. Hence, with respect to the GCE, the electroactive surface area for the MWCNT/GCE increases 1.9-fold and by 4.9-fold for NS-AC-MWCNT/GCE.

Sensor Optimization. The current at the redox peak for SWV conducted at 0.0002 V with varying amounts of NS-AC-MWCNT deposited on the GCE increases with increasing amounts of NS-AC-MWCNT, as shown in Figure S2, which can be attributed to the increase in surface coverage of the bare electrode. The current reaches a maximum for a 15 μL deposition volume, but for larger depositions, the response remains virtually the same. Hence, the 15 μL deposition volume is selected for all further experiments.

The effect of varying the pH of acetate buffer solution from 3 to 6 on the peak current and peak oxidation potential is next investigated using SWV, as shown in Figure 5. Increasing the pH from 3 to 5 increases the current at the peak oxidation potential for the redox couple, but above pH = 5, this current decreases with increasing pH, as seen in Figure 5A. The lowering of current is attributed to the decrease in the proton concentration required to reduce the −NO group of FT.[50] Thus, pH = 5 is identified as the optimum acidity for our investigation. In a 50 μM FT sample, the peak oxidation potential becomes negative as the acetate buffer pH increases due to proton participation in the oxidation of −NHOH to −NO.[22] Figure 4B shows a linear relationship between the peak oxidation potential and solution pH of the form peak potential (V) = −0.0569 pH + 0.2877 with R^2 = 0.9937 and a 56.9 mV pH^{-1} slope, indicating equal 1:1 contributions from protons and electrons during the electrochemical reaction of FT.[21,22,51]

The accumulation potential V_{pp} and accumulation time t_{pp} are relevant when an analyte reaction, i.e., of FT, is adsorption-controlled. The influence of these parameters on the Faradaic current response is investigated by varying V_{pp} from −0.5 to −0.8 V vs Ag/AgCl and t_{pp} from 40 to 140 s with magnetic stirring of the solution. Figure S3A shows that peak current increases as V_{pp} (applied at t_{pp} = 30 s) increases from −0.5 to −0.6 V vs Ag/AgCl, followed by a decrease in current when V_{pp} is further increased to −0.8 V vs Ag/AgCl. Consequently, −0.6 V vs Ag/AgCl (Figure S3B) is selected as the optimum V_{pp} for FT detection with SWV. The effect of t_{pp} on the peak current at −0.6 V vs Ag/AgCl is shown in Figure S3C, where the current saturates at t_{pp} = 100 s (Figure S3D). Hence, we select V_{pp} = −0.6 V vs Ag/AgCl with t_{pp} = 100 s to develop the FT sensor.

The SWV parameters are optimized for current response and peak shape as shown in Figure S4. The frequency is varied between 5 and 25 Hz (Figure S4A) maintaining the step

https://doi.org/10.1021/acsanm.1c00376
ACS Appl. Nano Mater. 2021, 4, 4781−4789

Table 1. Voltametric Detection of Fenitrothion with Different Electrodes

electrode	technique	linear range (μM)	LOD (μM)	references
CeO_2/rGO/GCE	DPV[a]	0.025−2.0	0.003	52
RGO/DPA/PGE	SWV	0.096−1.912	0.00348	53
ZrO_2/rGO/MoS_2-Au/GCE	SWV	0.018−21.6	0.00794	16
AuNPs@GNIP-GR-IL/GCE	DPV[a]	0.010−5.0	0.008	54
nano-TiO_2/GCE	DPV[a]	0.025−10.0	0.010	55
PNT/PGE	SWV	0.114−1.172	0.0196	56
MWCNT/GCE	SWV	0.20−60.0	0.080	22
TiO_2/nafion/GCE	DPV[a]	0.20−4.0	0.0866	57
NS-AC-MWCNT/GCE	SWV	0.050−40.0	0.00491	this work

[a]DPV—differential pulse voltammetry.

potential and amplitude at 10 and 50 mV, respectively. The maximum current response occurs at 10 Hz (Figure S4B) and then decreases as the frequency increases. Hence, 10 Hz is selected as the optimal frequency to optimize the step potential that is varied between 2 and 20 mV (Figure S4C). The maximum current occurs at 10 mV (Figure S4D), which we set as the optimum step potential. As shown in Figure S4E, the current increases as the amplitude increases from 20 to 140 mV, following which it decreases slightly with further increases in the amplitude (Figure S4F). On this basis, the 140 mV amplitude at 10 Hz frequency and 10 mV step potential is selected to examine the SWV response toward FT.

Sensor Performance. The analytical sensitivity of the sensor is investigated by spiking different concentrations of FT in ABS, as shown in Figure 6A. The sensor response provides the calibration curve in Figure 6B (Table S2). The response is linear for 0.05−40 μM FT concentrations, where the peak current response I_{pc} (μA) = 5.09C (μM) + 26.38 with R^2 = 0.98. The LOD for FT is 4.91 nM for S/N = 3 based on three replicates for each concentration, n = 3. This performance is compared with previously reported results in Table 1. The analytical performance of the NS-AC-MWCNT-modified GCE sensor is comparable with CeO_2/rGO/GCE and RGO/DPA/PGE and better than that of several other sensors which are attributed to its larger electroactive surface area and higher electrical conductivity of NS-AC-MWCNT compared to MWCNT, AuNPs, TiO_2, and peptide nanotubes (PNT).

The selectivity of the NS-AC-MWCNT-modified GCE sensor is investigated by spiking organophosphates (dichlorvos and chlorpyrifos) and the salts of nine commonly found interferents in drinking or usable water, namely, Ni^{2+}, Zn^{2+}, Mn^{2+}, Co^{2+}, Fe^{3+}, Cl^-, PO_4^{3-}, NO_3^-, and SO_4^{3-} in FT-containing ABS. Figure 6C,D shows that a 10-fold excess concentration of any salt interferent above the FT concentration has a negligible effect on the Faradaic current for the optimized FT sensing conditions. The shape of the peak was observed to be influenced by the presence of interferents. It is suggested that interactions of ions with FT in solution likely influence the mass transport of FT and hence the kinetics of the electrode reactions. On the other hand, dichlorvos and particularly chlorpyrifos influence FT detection. The effect of the latter compound is attributed to passivation of the electrode surface due to chlorpyrifos adsorption, possibly through $\pi-\pi$ interactions between chlorpyrifos and the NS-AC-MWCNT/GCE. Overall, the results support the selective sensing ability of the sensor for detecting FT in contaminated water.

After confirming the sensitivity and selectivity of the NS-AC-MWCNT/GCE sensor, we explore its applicability for detecting FT in realistic lake and tap water samples spiked with known FT concentrations. The sensor reports FT concentrations that equal 86.4−90.6% of the spiked concentrations with a maximum RSD of 8.2% (number of replicates, n = 3) for lake water, where this recovery is a larger 91.2−97.9% for tap water with maximum RSD of 2.7% (n = 3), as reported in Table 2. The lower FT recovery for lake water is attributed to signal loss due to coadsorption of lake water components, consisting of microorganisms, heavy metal ions, and waste,[58] on the electrodes, leading to their subsequent passivation and fouling. Nevertheless, the sensor can detect FT in contaminated water bodies. Sensor stability was assessed by storing NS-AC-MWCNT/GCE for 6 days at 4 °C after which the sensor response toward 20 μM FT was 86.1% of the initial current response. Overall, the sensor exhibits excellent reproducibility since the RSD is lower than 5% for all FT concentrations in the 0.05−40 μM range.

Table 2. Recovery of Various Concentrations of Spiked Fenitrothion in Lake and Tap Water (n = 3, Where n Is the Number of Replicates for Each of the Spiked FT Concentration)

sample type	spiked fenitrothion concentration (μM)	found (μM)	recovery (%)
lake water	20	18.12 ± 1.07	90.6 ± 5.3
	10	8.94 ± 0.74	89.4 ± 7.4
	5	4.32 ± 0.41	86.4 ± 8.2
tap water	20	19.51 ± 0.28	97.5 ± 1.4
	10	9.12 ± 0.27	91.2 ± 2.7
	5	4.89 ± 0.10	97.9 ± 2.0

CONCLUSIONS

We describe the facile fabrication of an effective, simple, and rapid electrochemical sensor to detect fenitrothion. A novel NS-AC-MWCNT composite is synthesized for use as the sensing material. The charge transfer resistance of the NS-AC-MWCNT/GCE electrode is 5.4 Ω compared to 12.6 Ω of the MWCNT/GCE electrode. The amorphous coating of activated carbon around the nanotube composite has a spongelike porous microstructure, which increases the overall surface area. Compared with GCE, MWCNT/GCE, and other reported electrodes, the NS-AC-MWCNT/GCE electrode has a higher sensitivity of FT detection, as low as 4.91 nM with a signal-to-noise ratio of 3. Tenfold concentrations of interferent salts of Ni^{2+}, Zn^{2+}, Mn^{2+}, Co^{2+}, Fe^{3+}, Cl^-, PO_4^{3-}, NO_3^-, and SO_4^{3-} and organophosphates (dichlorvos and chlorpyrifos) above the FT concentration do not have a significant effect on

https://doi.org/10.1021/acsanm.1c00376
ACS Appl. Nano Mater. 2021, 4, 4781−4789

its detection. With 5 μM FT spiked samples, the sensor satisfactorily recovers 86.4 ± 8.2% of FT in real lake and 97.9 ± 2.0% in tap water samples.

■ ASSOCIATED CONTENT

Supporting Information

The Supporting Information is available free of charge at https://pubs.acs.org/doi/10.1021/acsanm.1c00376.

Schematic of electrochemical reactions; XPS characterization; optimization of NS-AC-MWCNT ink deposition, accumulation potential, accumulation time, SWV parameters; and raw data for different FT concentrations used in the calibration plot (PDF)

■ AUTHOR INFORMATION

Corresponding Author

Ishwar K. Puri − *Department of Engineering Physics, McMaster University, Hamilton, Ontario L8S 4L7, Canada; Department of Mechanical Engineering and Department of Materials Science and Engineering, McMaster University, Hamilton, Ontario L8S 4L7, Canada;* orcid.org/0000-0002-8713-4188; Email: ikpuri@mcmaster.ca

Authors

Krishna Jangid − *Department of Engineering Physics, McMaster University, Hamilton, Ontario L8S 4L7, Canada;* orcid.org/0000-0003-3603-3982

Rakesh P. Sahu − *Department of Mechanical Engineering and Department of Materials Science and Engineering, McMaster University, Hamilton, Ontario L8S 4L7, Canada;* orcid.org/0000-0003-2443-6741

Richa Pandey − *Department of Engineering Physics, McMaster University, Hamilton, Ontario L8S 4L7, Canada*

Ri Chen − *Department of Mechanical Engineering, McMaster University, Hamilton, Ontario L8S 4L7, Canada*

Igor Zhitomirsky − *Department of Materials Science and Engineering, McMaster University, Hamilton, Ontario L8S 4L7, Canada*

Complete contact information is available at: https://pubs.acs.org/10.1021/acsanm.1c00376

Notes

The authors declare no competing financial interest.

■ ACKNOWLEDGMENTS

This work was supported by the Natural Sciences and Engineering Research Council of Canada (NSERC) Discovery Grant (RGPIN-2019-06571). The authors thank Dr. Carmen Andrei of Canadian Centre for Electron Microscopy for SEM and TEM, Dr. Zeynel Bayindir of Biointerfaces Institute for XPS and Ramis Arbi for Raman Spectroscopy.

■ REFERENCES

(1) Aktar, M. W.; Sengupta, D.; Chowdhury, A. Impact of pesticides use in agriculture: their benefits and hazards. *Interdiscip. Toxicol.* **2009**, *2*, 1−12.

(2) Hsu, J. P.; Wheeler, H. G., Jr.; Camann, D. E.; Schattenberg, H. J., III; Lewis, R. G.; Bond, A. E. Analytical Methods for Detection of Nonoccupational Exposure to Pesticides. *J. Chromatogr. Sci.* **1988**, *26*, 181−189.

(3) Ciucu, A.; Negulescu, C.; P Baldwin, R. Detection of pesticides using an amperometric biosensor based on ferophthalocyanine chemically modified carbon paste electrode and immobilized bienzymatic system. *Biosens. Bioelectron.* **2003**, *18*, 303−310.

(4) Vallero, D. A.; Letcher, T. M. *Unraveling Environmental Disasters*; Newnes, 2012.

(5) Mulchandani, A.; Chen, W.; Mulchandani, P.; Wang, J.; Rogers, K. R. Biosensors for direct determination of organophosphate pesticides. *Biosens. Bioelectron.* **2001**, *16*, 225−230.

(6) Parham, H.; Rahbar, N. Square wave voltammetric determination of methyl parathion using ZrO2-nanoparticles modified carbon paste electrode. *J. Hazard. Mater.* **2010**, *177*, 1077−1084.

(7) Liu, G.; Lin, Y. Electrochemical Sensor for Organophosphate Pesticides and Nerve Agents Using Zirconia Nanoparticles as Selective Sorbents. *Anal. Chem.* **2005**, *77*, 5894−5901.

(8) Wright, A. Rethinking the Circle of Poison: The Politics of Pesticide Poisoning among Mexican Farm Workers. *Latin Am. Perspect.* **1986**, *13*, 26−59.

(9) Pimentel, D. Environmental and economic costs of the application of pesticides primarily in the United States. *Environ. Dev. Sustainability* **2005**, *7*, 229−252.

(10) Tuan, S.-J.; Tsai, H.-M.; Hsu, S.-M.; Li, H.-P. Multiresidue analysis of 176 pesticides and metabolites in pre-harvested fruits and vegetables for ensuring food safety by gas chromatography and high performance liquid chromatography. *J. Food Drug Anal.* **2009**, *17*, 163−177.

(11) Sherma, J.; Zweig, G. Pesticides. *Anal. Chem.* **1985**, *57*, 1−15.

(12) Du, D.; Ye, X.; Zhang, J.; liu, D. Cathodic electrochemical analysis of methyl parathion at bismuth-film-modified glassy carbon electrode. *Electrochim. Acta* **2008**, *53*, 4478−4484.

(13) Upadhyay, S.; Rao, G. R.; Sharma, M. K.; Bhattacharya, B. K.; Rao, V. K.; Vijayaraghavan, R. Immobilization of acetylcholineesterase−choline oxidase on a gold−platinum bimetallic nanoparticles modified glassy carbon electrode for the sensitive detection of organophosphate pesticides, carbamates and nerve agents. *Biosens. Bioelectron.* **2009**, *25*, 832−838.

(14) Mahmoudi, E.; Fakhri, H.; Hajian, A.; Afkhami, A.; Bagheri, H. High-performance electrochemical enzyme sensor for organophosphate pesticide detection using modified metal-organic framework sensing platforms. *Bioelectrochemistry* **2019**, *130*, No. 107348.

(15) Li, H.; Wang, Z.; Wu, B.; Liu, X.; Xue, Z.; Lu, X. Rapid and sensitive detection of methyl-parathion pesticide with an electropolymerized, molecularly imprinted polymer capacitive sensor. *Electrochim. Acta* **2012**, *62*, 319−326.

(16) Qi, P.; Wang, J.; Wang, X.; Wang, X.; Wang, Z.; Xu, H.; Di, S.; Wang, Q.; Wang, X. Sensitive determination of fenitrothion in water samples based on an electrochemical sensor layered reduced graphene oxide, molybdenum sulfide (MoS2)-Au and zirconia films. *Electrochim. Acta* **2018**, *292*, 667−675.

(17) Zhu, W.; Liu, W.; Li, T.; Yue, X.; Liu, T.; Zhang, W.; Yu, S.; Zhang, D.; Wang, J. Facile green synthesis of graphene-Au nanorod nanoassembly for on-line extraction and sensitive stripping analysis of methyl parathion. *Electrochim. Acta* **2014**, *146*, 419−428.

(18) Khan, I.; Pandit, U. J.; Wankar, S.; Das, R.; Limaye, S. N. Fabrication of electrochemical nanosensor based on polyaniline film-coated AgNP-MWCNT-modified GCE and its application for trace analysis of fenitrothion. *Ionics* **2017**, *23*, 1293−1308.

(19) Canevari, T. C.; Prado, T. M.; Cincotto, F. H.; Machado, S. A. Immobilization of ruthenium phthalocyanine on silica-coated multiwall partially oriented carbon nanotubes: electrochemical detection of fenitrothion pesticide. *Mater. Res. Bull.* **2016**, *76*, 41−47.

(20) Arduini, F.; Cinti, S.; Scognamiglio, V.; Moscone, D. Nanomaterials in electrochemical biosensors for pesticide detection: advances and challenges in food analysis. *Microchim. Acta* **2016**, *183*, 2063−2083.

(21) Tefera, M.; Admassie, S.; Tessema, M.; Mehretie, S. Electrochemical sensor for determination of fenitrothion at multiwall carbon nanotubes modified glassy carbon electrode. *Anal. Bioanal. Chem. Res.* **2015**, *2*, 139−150.

(22) Salehzadeh, H.; Ebrahimi, M.; Nematollahi, D.; Salarian, A. A. Electrochemical study of fenitrothion and bifenox and their

simultaneous determination using multiwalled carbon nanotube modified glassy carbon electrode. *J. Electroanal. Chem.* **2016**, *767*, 188−194.
(23) Madhu, R.; Sankar, K. V.; Chen, S.-M.; Selvan, R. K. Eco-friendly synthesis of activated carbon from dead mango leaves for the ultrahigh sensitive detection of toxic heavy metal ions and energy storage applications. *RSC Adv.* **2014**, *4*, 1225−1233.
(24) Lee, J.; Kim, J.; Hyeon, T. Recent Progress in the Synthesis of Porous Carbon Materials. *Adv. Mater.* **2006**, *18*, 2073−2094.
(25) Lota, G.; Grzyb, B.; Machnikowska, H.; Machnikowski, J.; Frackowiak, E. Effect of nitrogen in carbon electrode on the supercapacitor performance. *Chem. Phys. Lett.* **2005**, *404*, 53−58.
(26) Guo, H.; Gao, Q. Boron and nitrogen co-doped porous carbon and its enhanced properties as supercapacitor. *J. Power Sources* **2009**, *186*, 551−556.
(27) Rennie, A.; Hall, P. Nitrogen-enriched carbon electrodes in electrochemical capacitors: Investigating accessible porosity using CM-SANS. *Phys. Chem. Chem. Phys.* **2013**, *15*, 16774−16778.
(28) Hulicova-Jurcakova, D.; Seredych, M.; Lu, G. Q.; Kodiweera, N. K. A. C.; Stallworth, P. E.; Greenbaum, S.; Bandosz, T. J. Effect of surface phosphorus functionalities of activated carbons containing oxygen and nitrogen on electrochemical capacitance. *Carbon* **2009**, *47*, 1576−1584.
(29) Wang, H.; Shao, Y.; Mei, S.; Lu, Y.; Zhang, M.; Sun, J.-k.; Matyjaszewski, K.; Antonietti, M.; Yuan, J. Polymer-derived heteroatom-doped porous carbon materials. *Chem. Rev.* **2020**, *120*, 9363−9419.
(30) Shi, K.; Ren, M.; Zhitomirsky, I. Activated carbon-coated carbon nanotubes for energy storage in supercapacitors and capacitive water purification. *ACS Sustainable Chem. Eng.* **2014**, *2*, 1289−1298.
(31) Shi, K.; Zhitomirsky, I. Asymmetric Supercapacitors Based on Activated-Carbon-Coated Carbon Nanotubes. *ChemElectroChem* **2015**, *2*, 396−403.
(32) He, Y.; Han, X.; Du, Y.; Song, B.; Zhang, B.; Zhang, W.; Xu, P. Conjugated polymer-mediated synthesis of sulfur-and nitrogen-doped carbon nanotubes as efficient anode materials for sodium ion batteries. *Nano Res.* **2018**, *11*, 2573−2585.
(33) Zhu, Y.; Shi, K.; Zhitomirsky, I. Anionic dopant−dispersants for synthesis of polypyrrole coated carbon nanotubes and fabrication of supercapacitor electrodes with high active mass loading. *J. Mater. Chem. A* **2014**, *2*, 14666−14673.
(34) Li, J. Conducting Polymer-based Electrodes for Electrochemical Supercapacitors, M.A.Sc Dissertation, McMaster University, Hamilton, ON, 2017. http://hdl.handle.net/11375/22172 (accessed 2021-05-04).
(35) Chen, R.; Puri, I.; Zhitomirsky, I. Polypyrrole-Carbon Nanotube-FeOOH Composites for Negative Electrodes of Asymmetric Supercapacitors. *J. Electrochem. Soc.* **2019**, *166*, A935.
(36) Su, Y.; Zhitomirsky, I. Asymmetric electrochemical supercapacitor, based on polypyrrole coated carbon nanotube electrodes. *Appl. Energy* **2015**, *153*, 48−55.
(37) Marie, M.; Mandal, S.; Manasreh, O. An electrochemical glucose sensor based on zinc oxide nanorods. *Sensors* **2015**, *15*, 18714−18723.
(38) Lehman, J. H.; Terrones, M.; Mansfield, E.; Hurst, K. E.; Meunier, V. Evaluating the characteristics of multiwall carbon nanotubes. *Carbon* **2011**, *49*, 2581−2602.
(39) Endo, M.; Takeuchi, K.; Hiraoka, T.; Furuta, T.; Kasai, T.; Sun, X.; Kiang, C.-H.; Dresselhaus, M. Stacking nature of graphene layers in carbon nanotubes and nanofibres. *J. Phys. Chem. Solids* **1997**, *58*, 1707−1712.
(40) Yang, M.; Cheng, B.; Song, H.; Chen, X. Preparation and electrochemical performance of polyaniline-based carbon nanotubes as electrode material for supercapacitor. *Electrochim. Acta* **2010**, *55*, 7021−7027.
(41) Hulicova-Jurcakova, D.; Seredych, M.; Lu, G. Q.; Bandosz, T. J. Combined effect of nitrogen-and oxygen-containing functional groups of microporous activated carbon on its electrochemical performance in supercapacitors. *Adv. Funct. Mater.* **2009**, *19*, 438−447.
(42) Ganesan, P.; Sivanantham, A.; Shanmugam, S. Inexpensive electrochemical synthesis of nickel iron sulphides on nickel foam: super active and ultra-durable electrocatalysts for alkaline electrolyte membrane water electrolysis. *J. Mater. Chem. A* **2016**, *4*, 16394−16402.
(43) Sadri, R.; Hosseini, M.; Kazi, S.; Bagheri, S.; Zubir, N.; Solangi, K.; Zaharinie, T.; Badarudin, A. A bio-based, facile approach for the preparation of covalently functionalized carbon nanotubes aqueous suspensions and their potential as heat transfer fluids. *J. Colloid Interface Sci.* **2017**, *504*, 115−123.
(44) Das, A.; Pisana, S.; Chakraborty, B.; Piscanec, S.; Saha, S. K.; Waghmare, U. V.; Novoselov, K. S.; Krishnamurthy, H. R.; Geim, A. K.; Ferrari, A. C.; Sood, A. K. Monitoring dopants by Raman scattering in an electrochemically top-gated graphene transistor. *Nat. Nanotechnol.* **2008**, *3*, 210−215.
(45) Ra, E. J.; An, K. H.; Kim, K. K.; Jeong, S. Y.; Lee, Y. H. Anisotropic electrical conductivity of MWCNT/PAN nanofiber paper. *Chem. Phys. Lett.* **2005**, *413*, 188−193.
(46) Maitra, T.; Sharma, S.; Srivastava, A.; Cho, Y.-K.; Madou, M.; Sharma, A. Improved graphitization and electrical conductivity of suspended carbon nanofibers derived from carbon nanotube/polyacrylonitrile composites by directed electrospinning. *Carbon* **2012**, *50*, 1753−1761.
(47) Bard, A. J.; Faulkner, L. R. Fundamentals and applications. *Electrochem. Methods* **2001**, *2*, 580−632.
(48) Ghadimi, H.; Tehrani, R. M.; Ali, A. S. M.; Mohamed, N.; Ab Ghani, S. Sensitive voltammetric determination of paracetamol by poly (4-vinylpyridine)/multiwalled carbon nanotubes modified glassy carbon electrode. *Anal. Chim. Acta* **2013**, *765*, 70−76.
(49) Yazdanparast, S.; Benvidi, A.; Abbasi, S.; Rezaeinasab, M. Enzyme-based ultrasensitive electrochemical biosensor using poly (l-aspartic acid)/MWCNT bio-nanocomposite for xanthine detection: a meat freshness marker. *Microchem. J.* **2019**, *149*, No. 104000.
(50) Geremedhin, W.; Amare, M.; Admassie, S. Electrochemically pretreated glassy carbon electrode for electrochemical detection of fenitrothion in tap water and human urine. *Electrochim. Acta* **2013**, *87*, 749−755.
(51) Shams, N.; Lim, H. N.; Hajian, R.; Yusof, N. A.; Abdullah, J.; Sulaiman, Y.; Ibrahim, I.; Huang, N. M. Electrochemical sensor based on gold nanoparticles/ethylenediamine-reduced graphene oxide for trace determination of fenitrothion in water. *RSC Adv.* **2016**, *6*, 89430−89439.
(52) Ensafi, A. A.; Noroozi, R.; Zandi, N.; Rezaei, B. Cerium (IV) oxide decorated on reduced graphene oxide, a selective and sensitive electrochemical sensor for fenitrothion determination. *Sens. Actuators, B* **2017**, *245*, 980−987.
(53) Surucu, O.; Bolat, G.; Abaci, S. Electrochemical behavior and voltammetric detection of fenitrothion based on a pencil graphite electrode modified with reduced graphene oxide (RGO)/poly (E)-1-(4-((4-(phenylamino) phenyl) diazenyl) phenyl) ethanone (DPA) composite film. *Talanta* **2017**, *168*, 113−120.
(54) Zhao, L.; Zhao, F.; Zeng, B. Synthesis of water-compatible surface-imprinted polymer via click chemistry and RAFT precipitation polymerization for highly selective and sensitive electrochemical assay of fenitrothion. *Biosens. Bioelectron.* **2014**, *62*, 19−24.
(55) Li, C.; Wang, C.; Ma, Y.; Hu, S. Voltammetric determination of trace amounts of fenitrothion on a novel nano-TiO 2 polymer film electrode. *Microchim. Acta* **2004**, *148*, 27−33.
(56) Bolat, G.; Abaci, S.; Vural, T.; Bozdogan, B.; Denkbas, E. B. Sensitive electrochemical detection of fenitrothion pesticide based on self-assembled peptide-nanotubes modified disposable pencil graphite electrode. *J. Electroanal. Chem.* **2018**, *809*, 88−95.
(57) Kumaravel, A.; Chandrasekaran, M. A biocompatible nano TiO2/nafion composite modified glassy carbon electrode for the detection of fenitrothion. *J. Electroanal. Chem.* **2011**, *650*, 163−170.
(58) Bhateria, R.; Jain, D. Water quality assessment of lake water: a review. *Sustainable Water Resour. Manage.* **2016**, *2*, 161−173.

https://doi.org/10.1021/acsanm.1c00376
ACS Appl. Nano Mater. 2021, 4, 4781−4789